

---

# Multimodal 3D Genome Pre-training

---

Minghao Yang<sup>1</sup> Pengteng Li<sup>1</sup> Yan Liang<sup>2</sup> Qianyi Cai<sup>1</sup> Zhihang Zheng<sup>3</sup> Shichen Zhang<sup>3</sup> Pengfei Zhang<sup>1</sup>  
Zhi-An Huang<sup>4</sup> Hui Xiong<sup>1</sup>

## Abstract

Deep learning techniques have driven significant progress in various analytical tasks within 3D genomics in computational biology. However, a holistic understanding of 3D genomics knowledge remains underexplored. Here, we propose **MIX-HIC**, the first multimodal foundation model of 3D genome that integrates both 3D genome structure and epigenomic tracks, which obtains unified and comprehensive semantics. For accurate heterogeneous semantic fusion, we design the cross-modal interaction and mapping blocks for robust unified representation, yielding the accurate aggregation of 3D genome knowledge. Besides, we introduce the first large-scale dataset comprising over **1 million** pairwise samples of Hi-C contact maps and epigenomic tracks for high-quality pre-training, enabling the exploration of functional implications in 3D genomics. Extensive experiments show that MIX-HIC can significantly surpass existing state-of-the-art methods in diverse downstream tasks. This work provides a valuable resource for advancing 3D genomics research.

## 1. Introduction

The three-dimensional (3D) organization of chromosomes within the nucleus plays a pivotal role in gene regulation and cellular function (Zhang et al., 2024; Monteagudo-Sánchez et al., 2024). Key topological features of 3D genome, such as chromatin loops, are essential for cell-type-specific transcriptional regulation. High-resolution 3D chromatin interactions can be quantified through high-throughput chromo-

some conformation capture (Hi-C) technique (Lieberman-Aiden et al., 2009). Understanding the mechanisms of how the 3D genome influences gene expression can unveil pivotal insights into cellular functionality, developmental biology, and disease mechanisms (Ferrer & Dimitrova, 2024).

Recently, computational models have emerged as a powerful tool to unravel the intricate associations between the 3D chromatin structure, epigenome, and transcriptome. Existing approaches predict various genomic features, including 3D chromatin contact maps (Yang et al., 2023; Tan et al., 2023; Fudenberg et al., 2020), chromatin loops (Salameh et al., 2020; Matthey-Doret et al., 2020; Wang et al., 2022), and gene expression (Zhang et al., 2023; Karbalayghareh et al., 2022), often leveraging DNA sequences, Hi-C contact maps and epigenomic tracks. Though success, most of these methods are limited to a single specific task and struggle to integrate the diverse and heterogeneous information of the 3D genome, hindering a comprehensive understanding of its complex organization.

Recent progress in large-scale foundation models have demonstrated remarkable success in various fields of computations biology, such as molecular representations (Feng et al., 2024; Chang & Ye, 2024), proteomics (Zhao et al., 2024; Gong et al., 2024), and genomics (Li et al., 2024; Schiff et al., 2024). Inspired by these advancements, we aim to develop a multimodal foundation model to address the above-mentioned limitations of analyzing 3D genomic downstream tasks in isolation.

Modeling the multimodal foundation model of 3D genome introduces three key challenges. First, Hi-C contact maps and epigenomic tracks have inherently distinct characteristics, making integration difficult. Simply aligning features from the two modalities and projecting them into a unified latent space would primarily capture modal-invariant knowledge like gene regulatory mechanisms, which are governed by both chromatin spatial organization and epigenomic tracks. However, this approach tends to overlook modal-specific characteristics, such as precise chemical modifications and chromatin states revealed by epigenomic tracks, which are essential factors for fine-grained 3D genome analysis. This can lead to information loss and degrade downstream task performance (Refer to Appendix B for theo-

<sup>1</sup>Artificial Intelligence Thrust, Information Hub, Hong Kong University of Science and Technology (Guangzhou), Guangzhou, 511466, China <sup>2</sup>School of Artificial Intelligence, South China Normal University, Foshan, 528225, China <sup>3</sup>Bioscience and Biomedical Engineering Thrust, System Hub, Hong Kong University of Science and Technology (Guangzhou), Guangzhou, 511466, China <sup>4</sup>Research Office, City University of Hong Kong (Dongguan), Dongguan 523000, China. Correspondence to: Zhi-An Huang <huang.za@cityu-dg.edu.cn>, Hui Xiong <xionghui@ust.hk>.

*retical analysis*). Second, the unified representation from heterogeneous 3D genomic and epigenomic data must exhibit robust generalization capabilities, otherwise, the model may struggle to adapt effectively to diverse downstream tasks *e.g.*, generation and regression. Third, uncovering implicit semantic relationships between 3D genomic and epigenomic data is crucial for addressing the data scarcity problem in 3D genomics. Especially, the high experimental costs of Hi-C sequencing in real-world applications limit data accessibility, leading to incomplete representations and degraded model performance. Pre-training a model to learn implicit multimodal structural connections offers significant benefits for downstream tasks, particularly when only single-modality data is available. This enables the model to leverage structural knowledge to compensate for missing modality semantics, thereby enriching the overall data representation.

Hence, we introduce MIX-HIC, the first multimodal foundation model for 3D genomics to extract fine-grained knowledge from 3D genome and epigenomic tracks, enabling efficient adaptation to diverse downstream tasks with superior performance. Specifically, MIX-HIC first incorporates two distinct encoders to capture the refined features from 3D genome contact maps and epigenomic tracks, leveraging cell type-specific information for accurate predictions in novel cell types. To address the challenge of integrating heterogeneous data, we propose a cross-modal interaction block to capture both modal-invariant and modal-specific representations, regularized by contrastive learning and orthogonal constraints, preserving both shared and distinctive information across modalities. Additionally, a cross-modal mapping block facilitates information exchange between modalities, ensuring robust representation even with single-modality input. To comprehensively capture 3D genome knowledge, we have curated a large-scale dataset which consists of 1,275,948 pair samples of Hi-C contact maps and epigenomic tracks for rapid adaptation to downstream tasks through task-specific decoders. Notably, this is the largest paired dataset for the 3D genome analysis to date. MIX-HIC is evaluated across diverse downstream tasks, demonstrating its effectiveness and robustness in comparison to other state-of-the-art methods. In summary, the main contributions are:

- We propose *the first 3D genomic multimodal foundation model*, integrating Hi-C contact maps and epigenomic tracks to establish a new paradigm for 3D genome analysis.
- MIX-HIC features a novel architecture with two key components: (1) a cross-modal interaction block to capture both shared and unique biological patterns across modalities; and (2) a cross-modal mapping block to enable a reliable complement of missing modality fea-

tures.

- For holistic representation learning for 3D genome analysis, we present *the largest paired dataset of Hi-C and epigenomic tracks*, comprising over 1 million samples.
- Extensive experiments demonstrate that MIX-HIC achieves state-of-the-art performance on three critical downstream tasks across two cell lines.

## 2. Related Works

### 2.1. 3D Genome-Related Tasks

This work evaluates the effectiveness of MIX-HIC on three downstream tasks, including Hi-C contact maps prediction, chromatin loops prediction, and CAGE-seq expression prediction.

Existing methods for Hi-C contact maps prediction from DNA sequences show promise but lack cross-cell-type generalization (Fudenberg et al., 2020; Schwessinger et al., 2020). Models like EPCOT (Zhang et al., 2023) and C.Origami (Tan et al., 2023) improve this by integrating DNA sequence with cell-type-specific epigenomic tracks. Epiphany (Yang et al., 2023) offers a more efficient solution using only the epigenomic tracks.

Chromatin loop prediction methods are broadly divided into statistical and supervised learning methods. Statistical methods like HiCExplorer (Wolff et al., 2020) and ChromoSight (Matthey-Doret et al., 2020) rely on contact frequency distributions or expert-defined templates to identify loops. Supervised learning methods, including Peakachu (Salameh et al., 2020), DLoopCaller (Wang et al., 2022) leverage labeled data and sophisticated architectures for loop prediction. RefHiC (Zhang & Blanchette, 2023) employs a coarse-to-fine training strategy that integrates multi-resolution Hi-C contact maps through contrastive learning mechanisms for model pre-training. However, RefHiC is limited by its reliance on small-scale data semantics, which hinders its generalizability to other downstream tasks in 3D genome.

CAGE-seq expression prediction typically uses multimodal inputs, including DNA sequences, epigenomic tracks, and Hi-C contact maps. Enformer (Avsec et al., 2021) employs transformers for modeling DNA sequences, while EPCOT (Zhang et al., 2023) integrates DNA sequences and epigenomic tracks with transformers or long short-term memory (LSTM) (Hochreiter, 1997). GraphReg (Karbalayghareh et al., 2022) integrates epigenomic tracks and Hi-C contact maps using graph attention networks for expression prediction.

Despite their notable achievements, these methods often

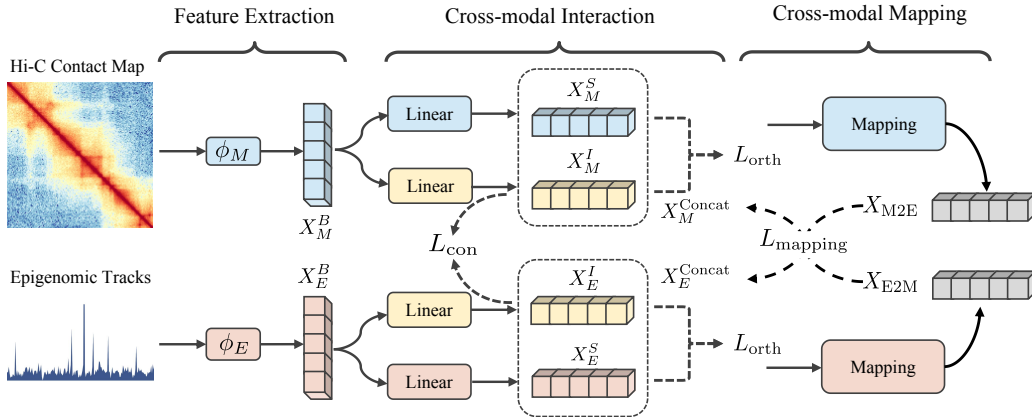


**Figure 1. Pre-training stage of MIX-HIC.** MIX-HIC employs a dual-encoder architecture to extract refined features from both Hi-C contact maps and epigenomic tracks. The modal-specific and modal-invariant representations are learned via contrastive learning and orthogonal constraints within the cross-modal interaction block. A cross-modal mapping block is developed to further regularize the bimodal representations and facilitate cross-modal complement.  $\phi_M$  and  $\phi_E$  denote the Hi-C contact map encoder and epigenomic track encoder, respectively.

**Table 1.** Summary of pre-training data for MIX-HIC, including original and cleaned data counts.

Cell line	Original	Cleaned	Remain
HepG2	48, 415	38, 536	79.5%
HCT116	276, 384	189, 099	68.4%
IMR90	471, 557	316, 794	67.2%
WTC11	1, 032, 048	731, 519	70.9%
<b>Total</b>	<b>1, 828, 401</b>	<b>1, 275, 948</b>	<b>69.8%</b>

exhibit limitations in knowledge transfer across tasks and fail to fully capture the complex interaction patterns between multimodal data.

## 2.2. Foundation Models in Computational Biology

The emergence of foundation models has significantly advanced various fields of computational biology. For example, EvoRank (Zhao et al., 2024) has demonstrated remarkable capabilities by harnessing extensive protein sequence datasets to derive latent representations through sequence alignment. VQDNA (Li et al., 2024) employs large-scale DNA sequences to learn adaptive tokenization through vector-quantized codebooks. To capture more comprehensive views of data, multimodal foundation models such as ESM-IF (Hsu et al., 2022) combine protein sequences and 3D structures to learn functional and structural representations, advancing protein function design and prediction. Similarly, UniCorn (Feng et al., 2024) integrates 2D and 3D molecular views through contrastive learning, effectively capturing complementary bimodal features. These foundation models have showcased strong representation learning capabilities of foundation models, inspiring the development of a universal model capable of effectively addressing various downstream tasks in the 3D genomic field.

## 3. Data Processing and Preparation

To distill the comprehensive semantics from the 3D genome, we collect and refine a large-scale dataset for pre-training MIX-HIC, using publicly available data from the hg38 assembly. The Hi-C contact maps are obtained from the 4DN Data Portal<sup>1</sup>, while the epigenomic tracks (ATAC-seq and DNase-seq), CAGE-seq expression data, and CTCF ChIA-PET (Li et al., 2010) chromatin loops are downloaded from the ENCODE Portal<sup>2</sup>. MIX-HIC processes 250,000 base pair (bp) genomic windows as input. The Hi-C contact maps are represented as  $50 \times 50$  matrices per window at 5 kb resolution, while epigenomic tracks are averaged over every 100 bps to reduce data variability, generating 2,500-length sequences. Each bin in the Hi-C matrix corresponds to specific  $x$  and  $y$  coordinates, representing two distinct genomic segments. Their respective epigenomic sequences are concatenated into a 5,000-length representation for that bin. Thus, Hi-C contact maps and epigenomic tracks are treated as images and sequences, respectively. We focus on four cell lines for pre-training, including HepG2, HCT116, IMR90, and WTC111. To ensure data quality, we filter out windows with fewer than 10% non-zero Hi-C interactions or insufficient contact signals. This process results in a total of 1,275,948 pairwise samples of Hi-C contact maps and epigenomic tracks within chromatin loop regions for pre-training. Table 1 summarizes the sample counts before and after this filtering process. *Further details on data processing, reference number, and downstream task data are provided in Appendix A.1.*

<sup>1</sup><https://data.4dnucleome.org/>

<sup>2</sup><https://www.encodeproject.org/>

## 4. Methodology

### 4.1. Self-supervised Pre-training

Self-supervised learning (Chen et al., 2020) offers a powerful solution for learning unified and comprehensive representations from heterogeneous 3D genomic and epigenomic data. By leveraging large-scale pairwise data during pre-training, MIX-HIC effectively captures inherent biological patterns and relationships across these bimodal data, significantly enhancing its adaptability to diverse downstream tasks. As shown in Figure 1, the pre-training phase includes a feature extraction block, cross-modal interaction block, and cross-modal mapping block. The feature extraction block employs specialized encoders for epigenomic tracks and Hi-C contact maps, respectively, to generate refined representations. The learned representations are then fed into the cross-modal interaction block to learn both modal-specific and modal-invariant features. This learning process is regularized through a combination of contrastive learning loss and orthogonal loss. Finally, a cross-modal mapping block further explores latent connections and complementary information between the two modalities.

**Feature extraction block.** The feature extraction block consists of Hi-C and epigenomic feature encoders. Given the Transformer’s capability to model long-range dependencies and its flexibility in capturing both spatial interactions (Hi-C contact maps) and sequential relationships (epigenomic tracks), we utilize a Transformer-based architecture for robust feature extraction and multimodal integration. Similar to Vision Transformer (ViT) (Dosovitskiy et al., 2021), the single-channel Hi-C contact map  $X_M \in \mathbb{R}^{1 \times H \times W}$  is first transformed into a sequence of flattened patches  $X_M^p \in \mathbb{R}^{N \times D}$ . Here,  $H$  and  $W$  are the height and width of the Hi-C contact map, both equal to 50. The dimension  $D = 1 \times P \times P$  corresponds to the initial size of each patch, where the patch size  $P$  is set to 2. The total number of these patches  $N = H \times W/P^2$  is the resulting number of patches, which becomes the input sequence length. In the Hi-C feature encoder, a feedforward network projects these patches into an embedding  $X_M^0 \in \mathbb{R}^{N \times C}$ , where  $C$  denotes the predefined feature dimension. This embedding is then refined through three cascaded encoder layers, where each layer consists of  $T$  Transformer blocks followed by a downsampling layer, yielding progressively refined embeddings  $X_M^i \in \mathbb{R}^{\alpha_i \times C_i}$ , where the sequence length  $\alpha_i$  is defined as  $\alpha_i = \frac{N}{4^i}$  and the feature dimension  $C_i$  grows exponentially as  $C_i = 2^i C$ , with the encoder layer  $i \in \{1, 2, 3\}$ . Finally, a bottleneck layer equipped with  $T$  Transformer blocks is applied to produce the Hi-C contact map embedding  $X_M^B \in \mathbb{R}^{\alpha_3 \times C_3}$ .

The epigenomic encoder processes input sequences  $X_E \in \mathbb{R}^{L_1 \times O}$ , where  $L_1 = 5,000$  is the initial sequence length, and  $O$  represents the two epigenomic tracks: ATAC-seq and

DNase-seq. Convolutional layers with max-pooling operations extract an initial embedding  $X_E^0 \in \mathbb{R}^{L_2 \times C}$ , where  $L_2 = 100$  corresponds to two genomic segments along both  $x$  and  $y$  axes in the Hi-C contact map. Similarly, the embedding  $X_E^0$  is processed through three encoder layers, where each layer consists of  $T$  Transformer blocks followed by a downsampling layer, resulting in  $X_E^i \in \mathbb{R}^{\beta_i \times C_i}$ , where the sequence length  $\beta_i = \frac{L_2}{2^i}$  for  $i \in \{1, 2, 3\}$ . Then, the refined epigenomic representation  $X_E^B \in \mathbb{R}^{\beta_3 \times C_3}$  is also derived from a final bottleneck layer.

**Cross-modal interaction block.** Conventional multimodal learning architectures (Yang et al., 2024) often utilize contrastive learning to project features from different modalities into a shared embedding space. However, these modalities inherently contain both homogeneous and heterogeneous information. Direct aligning all features risks losing essential modal-specific characteristics, potentially diminishing downstream task performance (Dong et al., 2023; Wang et al., 2023). *This is further analyzed in the Appendix B.*

To address this, our cross-modal interaction block captures both modal-specific and modal-invariant representations, enabling a more comprehensive understanding of the data. Specifically, we employ four independent dense networks to process the Hi-C contact map representation  $X_M^B$  and the epigenomic representation  $X_E^B$ . This generates the condensed modal-invariant representations  $X_M^I \in \mathbb{R}^{\alpha_3 \times C_2}$  and  $X_E^I \in \mathbb{R}^{\beta_3 \times C_2}$ , as well as the modal-specific representations  $X_M^S \in \mathbb{R}^{\alpha_3 \times C_2}$  and  $X_E^S \in \mathbb{R}^{\beta_3 \times C_2}$ . The mean pooling operation is then applied along the sequence length dimension, producing  $\hat{X}_M^I, \hat{X}_E^I, \hat{X}_M^S,$  and  $\hat{X}_E^S$ , each with a feature dimension of  $C_2$ . To ensure that the modal-invariant features capture shared knowledge across modalities, we incorporate a contrastive learning loss to regularize these representations. We propose a unified contrastive loss function  $\mathcal{L}_{\text{pair}}$  to compute the similarity between two modalities  $\mathcal{A}$  and  $\mathcal{B}$  as follows:

$$\mathcal{L}_{\text{pair}}(\mathcal{A}, \mathcal{B}) = -\frac{1}{J} \sum_{j=1}^J \log \frac{\exp\langle \mathcal{A}_j, \mathcal{B}_j \rangle / \tau}{\sum_{r=1}^J \exp\langle \mathcal{A}_j, \mathcal{B}_r \rangle / \tau}, \quad (1)$$

where  $\tau$  denotes the temperature, commonly set to 0.07 (Kim et al., 2023),  $J$  refers to the batch size,  $\langle \cdot, \cdot \rangle$  is the dot product operation, and  $\mathcal{A}_j$  and  $\mathcal{B}_j$  represent the embedding of the  $j$ -th sample in the mini-batch for modality  $\mathcal{A}$  and  $\mathcal{B}$ , respectively. Finally, the overall contrastive loss is computed as follows:

$$\mathcal{L}_{\text{con}} = \frac{1}{2} (\mathcal{L}_{\text{pair}}(\hat{X}_E^I, \hat{X}_M^I) + \mathcal{L}_{\text{pair}}(\hat{X}_M^S, \hat{X}_E^S)). \quad (2)$$

Moreover, we introduce orthogonal constraint to maximize the dissimilarity between modal-specific and their modal-invariant features. This ensures that the modal-specific features capture complementary information distinct from the

shared knowledge represented by the modal-invariant features. The orthogonal loss  $\mathcal{L}_{\text{orth}}$  is calculated by minimizing the inner product between these features as follows:

$$\mathcal{L}_{\text{orth}} = \frac{1}{2} \left( \langle \hat{X}_M^S, \hat{X}_M^I \rangle + \langle \hat{X}_E^S, \hat{X}_E^I \rangle \right). \quad (3)$$

**Cross-modal mapping block.** Data scarcity, often due to high experimental costs, can lead to incomplete datasets with missing modalities. Integrating predicted features of a missing modality with existing modalities can enhance prediction performance (Kim & Kim, 2025; Wang et al., 2023). Our cross-modal mapping block aims to capture the implicit semantic relationships and facilitate knowledge transfer between modalities to address this issue.

Some downstream tasks require the MIX-HIC to preserve the sequence length of the input features. However, the differing lengths of Hi-C contact maps and epigenomic tracks pose a challenge for effective modality transfer. Therefore, we apply 1D adaptive pooling to the concatenated representations of Hi-C,  $X_M^{\text{Concat}} = [X_M^I : X_M^S] \in \mathbb{R}^{\alpha_3 \times C_3}$  and epigenomic tracks,  $X_E^{\text{Concat}} = [X_E^I : X_E^S] \in \mathbb{R}^{\beta_3 \times C_3}$  (where  $[\cdot : \cdot]$  denotes concatenation), to align their lengths. This yields the complementary representations  $X_{M2E} \in \mathbb{R}^{\beta_3 \times C_3}$  and  $X_{E2M} \in \mathbb{R}^{\alpha_3 \times C_3}$  as follows:

$$X_{M2E} = \mathcal{F}_{M2E}(\mathcal{G}_{M2E}(X_M^{\text{Concat}})), \quad (4)$$

$$X_{E2M} = \mathcal{F}_{E2M}(\mathcal{G}_{E2M}(X_E^{\text{Concat}})), \quad (5)$$

where  $\mathcal{G}_{M2E}$  and  $\mathcal{G}_{E2M}$  are 1D adaptive pooling operations.  $\mathcal{F}_{M2E}$  and  $\mathcal{F}_{E2M}$  denote dense layers with the same output dimensions matching their inputs. To ensure these mapped embeddings capture the relevant information from the target modality, we use an  $\mathcal{L}_2$  constraint for regularization:

$$\mathcal{L}_{\text{mapping}} = \frac{1}{2} (\|X_{M2E} - X_E^{\text{Concat}}\|_2^2 + \|X_{E2M} - X_M^{\text{Concat}}\|_2^2). \quad (6)$$

Overall, the final loss for self-supervised pre-training is computed as follows:

$$\mathcal{L}_{\text{pretrain}} = \mathcal{L}_{\text{con}} + \mathcal{L}_{\text{orth}} + \mathcal{L}_{\text{mapping}}. \quad (7)$$

## 4.2. Task-specific Fine-tuning

As depicted in Figure 2, MIX-HIC is a versatile framework capable of processing various kinds of inputs. Ideally, MIX-HIC takes both the Hi-C contact map and the epigenomic feature profile as inputs, extracting their concatenated features  $X_M^{\text{Concat}}$  and  $X_E^{\text{Concat}}$  similar to the feature extraction block used in the self-supervised pre-training stage. However, in real-world scenarios, certain modality may be absent for various unforeseen reasons. Leveraging the powerful representation ability of pre-training to capture implicit connections between bimodal data, MIX-HIC incorporates a

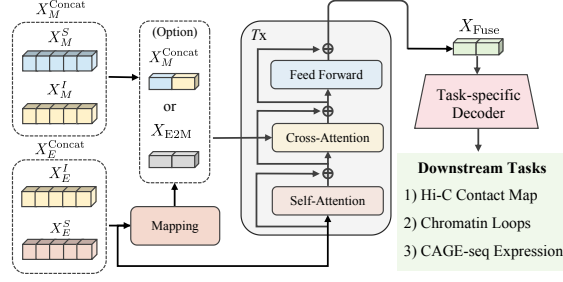


**Figure 2. Fine-tuning stage of MIX-HIC.** Epigenomic features are captured from the pre-trained encoder, while Hi-C contact map features are obtained either directly from the pre-trained encoder or through feature mapping based on the epigenomic features. MIX-HIC incorporates a modality fusion block to integrate the bimodal representations, followed by a task-specific decoder for final predictions of downstream tasks.

cross-modal mapping block to complement the features of the missing modality using the information from the available modality. For example, when the Hi-C contact map is missing, MIX-HIC can infer the missing modality features  $X_{E2M}$  from the concatenated epigenomic embedding  $X_E^{\text{Concat}}$  using Eq. 5. For the Hi-C contact map prediction task, even only the epigenomic tracks are available, the corresponding contact map features  $X_{E2M}$  can still be utilized for prediction.

**Modality-fusion block.** We employ  $T$  stacked contact map-grounded fusion blocks to learn the interaction patterns between the bimodal representations. Each contact map-grounded fusion block consists of a self-attention layer, a cross-attention layer, and a feedforward network. The extracted epigenomic embeddings  $X_E^{\text{Concat}}$  are first input into the self-attention layer, generating query embeddings of the cross-attention layer. The contact map embeddings, either  $X_M^{\text{Concat}}$  or  $X_{E2M}$ , serve as the key and value embeddings, which are then processed through the cross-attention layer. Finally, a feedforward neural network is applied to produce the fusion embeddings  $X_{\text{Fuse}} \in \mathbb{R}^{\beta_3 \times C_3}$ .

**Task-specific prediction block.** Three types of decoders are involved in the task-specific prediction block. The chromatin loop prediction task is a binary classification problem, where the goal is to classify a given sample as either a chromatin loop or a non-loop. Therefore, the decoder for this task includes a mean pooling operation along the sequence length axis, followed by a feedforward network.

The CAGE-seq expression task is formulated as a regression problem, aiming to predict 100 values corresponding to the expression levels of two genomic segments (each of length 50) along  $x$ -axis and  $y$ -axis of the Hi-C contact map. The decoder consists of three transformer blocks, with each followed by an upsampling layer. At each stage, the encoder-derived features  $X_E^i$  from the  $i$ -th encoder layer are concatenated with the corresponding  $i$ -th layer of de-

Table 2. Methods comparison for the Hi-C contact map prediction task on GM12878 and K562 cell lines. The results marked in **bold** and underlined denote the best and second-best performing methods, respectively.

Methods	GM12878		K562	
	PCC	$R^2$	PCC	$R^2$
Epiphany	0.9159	0.7970	0.8629	0.6547
C.Origami	0.9258	0.7958	0.8934	0.7055
EPCOT-LSTM	0.9376	<u>0.7993</u>	0.9111	<u>0.7840</u>
EPCOT-transformer	<u>0.9391</u>	0.5409	<u>0.9158</u>	0.7648
MIX-HIC-InferMap	<b>0.9441</b>	<b>0.8724</b>	<b>0.9181</b>	<b>0.8001</b>

coder outputs  $X_D^i$  from the preceding stage via skip connections, facilitating feature integration across network depths. Finally, the decoder output features  $X_{\text{out}} \in \mathbb{R}^{L_2 \times 2C}$  are processed through two feedforward networks to generate regression predictions.

To predict the  $50 \times 50$  Hi-C contact maps at 5kb resolution, the decoder output features  $X_{\text{out}}$  are obtained similar to the CAGE-seq expression task. These features are then split into two feature segments  $X_{\text{out}}^1 \in \mathbb{R}^{50 \times 2C}$  and  $X_{\text{out}}^2 \in \mathbb{R}^{50 \times 2C}$  along the length axis.  $X_{\text{out}}^1$  and  $X_{\text{out}}^2$  are unsqueezed into  $\mathbb{R}^{50 \times 1 \times 2C}$  and  $\mathbb{R}^{1 \times 50 \times 2C}$ , respectively, after which element-wise addition and multiplication operations are applied to generate feature maps of size  $\mathbb{R}^{50 \times 50 \times 2C}$ . Finally, two layers of feedforward networks are utilized to predict the Hi-C contact maps.

**Training loss.** The chromatin loop prediction task employs the binary cross entropy (BCE) loss function, while the Hi-C contact map prediction and CAGE-seq expression prediction tasks use the mean squared error (MSE) loss function. These loss functions can be formulated as follows:

$$\mathcal{L}_{\text{MSE}} = \frac{1}{J} \sum_{j=1}^J (y_j - \hat{y}_j)^2,$$

$$\mathcal{L}_{\text{BCE}} = -\frac{1}{J} \sum_{j=1}^J [y_j \log(\hat{y}_j) + (1 - y_j) \log(1 - \hat{y}_j)].$$
(8)

where  $y_i$  and  $\hat{y}_i$  represent the true value and the predicted value, respectively.

## 5. Experiments

*Implementation details and hyperparameter analysis can be referred to Appendix.*

### 5.1. Comparison Results on Downstream Tasks

To demonstrate the effectiveness of MIX-HIC, three downstream tasks are involved in this work, including Hi-C

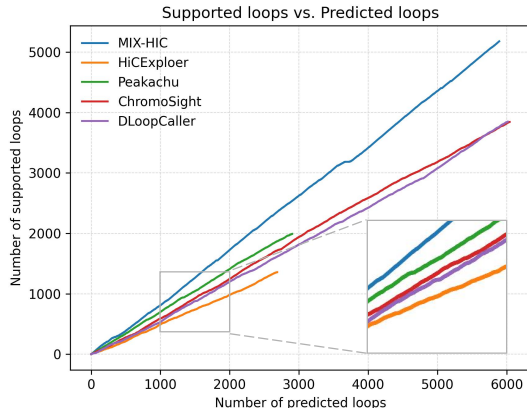


Figure 3. Comparison of the number of predicted loops with the number of ChIA-PET-supported loops across various deep learning methods on GM12878 cell line.

contact maps prediction, chromatin loops prediction, and CAGE-seq expression prediction.

**3D Chromatin Organization Prediction.** In this task, the Hi-C contact maps serve as the target. MIX-HIC-InferMap (a variant of MIX-HIC capable of inferring features of missing contact maps) is compared with four state-of-the-art methods, including Epiphany (Yang et al., 2023), C.Origami (Tan et al., 2023), and two variants of EPCOT (Zhang et al., 2023), (*i.e.* EPCOT-LSTM and EPCOT-transformer). For a fair comparison, all methods receive the same input as MIX-HIC and are configured with their default parameter settings. The coefficient of determination ( $R^2$ ) (Nagelkerke, 1991) and the Pearson correlation coefficient (PCC) (Cohen et al., 2009) are employed as evaluation metrics.

Table 2 shows the evaluation performance on GM12878 and K562 cell lines. Compared to other methods, MIX-HIC demonstrates superior performance, achieving the highest average  $R^2$  and PCC values on both GM12878 and K562 cell lines. Specifically, it outperforms the runner-up method by approximately 0.5%/9.1% in PCC/ $R^2$  on GM12878, and by about 0.3%/2.1% on K562, respectively. We note that the EPCOT variants deliver competitive performance, but they suffer from fluctuations across the two datasets. Through extensive pre-training on large-scale pairwise datasets, MIX-HIC effectively explores implicit semantic relationships between bimodal data, enabling robust compensation for missing modality semantics and achieving promising accuracy in Hi-C contact map prediction.

**Chromatin Loops Prediction.** Two supervised machine learning-based methods DLoopCaller (Wang et al., 2022) and Peakachu (Salameh et al., 2020) are used to compare with MIX-HIC-Bimodal (a variant of MIX-HIC combining both Hi-C contact maps and epigenomic tracks). As illustrated in Table 3, MIX-HIC surpasses other machine learning-based methods across most classification metrics

Table 3. Methods comparison for the supervised chromatin loops prediction task on GM12878 and K562 cell lines.

Methods	GM12878				K562			
	Precision	Recall	F1	AUROC	Precision	Recall	F1	AUROC
Peakachu	0.7763	<u>0.8283</u>	0.8015	0.8766	0.7857	<b>0.8062</b>	<u>0.7958</u>	0.8864
DLoopCaller	<b>0.8516</b>	0.8130	<u>0.8319</u>	<u>0.9118</u>	<u>0.8383</u>	0.7526	0.7932	<u>0.8924</u>
MIX-HIC-Bimodal	<u>0.8505</u>	<b>0.8337</b>	<b>0.8420</b>	<b>0.9209</b>	<b>0.8521</b>	<u>0.8027</u>	<b>0.8267</b>	<b>0.9194</b>

Table 4. Methods comparison for the CAGE-seq expression prediction task on GM12878 and K562 cell lines.

Methods	GM12878		K562	
	PCC	$R^2$	PCC	$R^2$
EPI-CNN	0.9213	0.7719	0.9354	0.8033
EPI-Graph	0.9200	0.7965	0.9256	0.8211
EPCOT-LSTM	0.8939	0.4723	<u>0.9359</u>	<u>0.8972</u>
EPCOT-transformer	<u>0.9337</u>	<u>0.8672</u>	0.8965	0.7744
MIX-HIC	<b>0.9435</b>	<b>0.8833</b>	<b>0.9569</b>	<b>0.9077</b>

on two datasets. By integrating both epigenomic tracks and Hi-C contact maps, DLoopCaller slightly outperforms Peakachu, which relies solely on Hi-C contact maps. The enhanced performance of MIX-HIC can be attributed to the effective self-supervised pre-training, which facilitates the capture of both modal-invariant and modal-specific information from bimodal representations, in contrast to the simple concatenation employed by DLoopCaller.

We employ both statistical-based methods, namely ChromoSight (Matthey-Doret et al., 2020) and HiCExplorer (Wolff et al., 2020), as well as machine learning-based methods to annotate loops across entire chromosomes. The predicted loops are further compared with those loops validated by experimental data from ChIA-PET. *Method details for whole-chromosome chromatin loop annotation and corresponding results are available in Appendix A.2 and C.1, respectively.* Figure 3 compares the number of predicted loops versus the number of loops supported by ChIA-PET among various methods on GM12878 dataset. Among all the methods, machine learning-based methods generally predict a higher number of loops that are validated by ChIA-PET on the GM12878 dataset, with MIX-HIC identifying the most ChIA-PET validated loops while maintaining the highest validated proportion. On the K562 dataset, which contains much less training data compared to GM12878, the efficacy of machine learning methods generally declines. Nevertheless, MIX-HIC consistently maintains the highest proportion of validated loops in comparison with other methods. *An example of whole-chromosome chromatin loop comparison is provided in Appendix C.2.*

**CAGE-seq Expression Prediction.** MIX-HIC is pitted against four benchmark methods: two variants of GraphReg

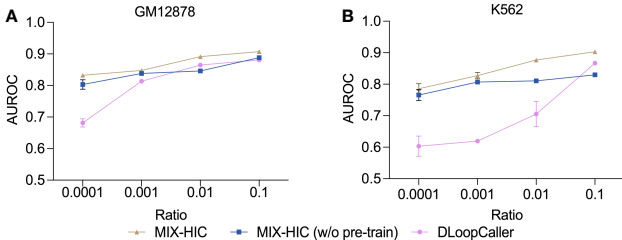


Figure 4. Few-shot chromatin loop classification performance across different training data ratios. Mean values and standard errors are calculated over five independent runs with varying random seeds.

(EPI-CNN and EPI-Graph) (Karbalayghareh et al., 2022), as well as two variants of EPCOT (EPCOT-LSTM and EPCOT-transformer) (Zhang et al., 2023). EPI-CNN relies solely on epigenomic tracks to predict CAGE-seq expression, whereas EPI-Graph enhances this approach by employing graph attention networks to integrate features from Hi-C contact maps, following the feature extraction of epigenomic tracks. Table 4 showcases the comparison results across two datasets. EPCOT achieves competitive performance, yet it suffers from a time-consuming problem due to the process of long-range DNA sequence. MIX-HIC demonstrates remarkable performance over other benchmark methods across all metrics on both datasets.

## 5.2. Few-shot Chromatin Loops Classification

We conduct a few-shot learning experiment on the chromatin loops classification task to evaluate the performance of MIX-HIC under limited training data scenarios. Specifically, we fine-tune MIX-HIC, a non-pre-trained variant of MIX-HIC, and DLoopCaller, using four different ratios of the training data, ranging from 0.0001 to 0.1. As illustrated in Figure 4, MIX-HIC consistently outperforms the non-pre-trained model and DLoopCaller across all data ratios, demonstrating the significant advantage of pre-training. DLoopCaller exhibits considerable performance fluctuations when the training data is limited. Notably, with a training data ratio of 0.1, MIX-HIC achieves an AUROC of approximately 0.9 on two datasets, which is competitive with other state-of-the-art methods trained on full datasets. These findings highlight the robustness and efficiency of

MIX-HIC in leveraging pre-trained knowledge to achieve superior performance even with limited labels.

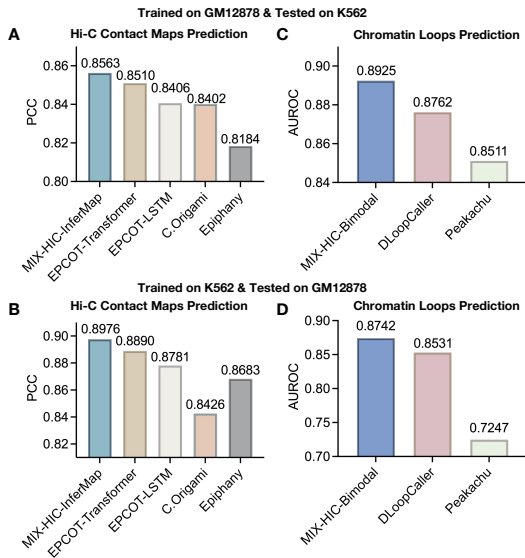


Figure 5. Cross-cell-type evaluation of MIX-HIC performance on Hi-C contact map prediction and chromatin loops prediction tasks.

### 5.3. Robust Performance Across Cell Types

The utilization of cell-type specific data, *i.e.*, Hi-C contact maps and epigenomic tracks, empowers MIX-HIC to achieve accurate predictions for novel cell types. We perform a cross-dataset evaluation with the GM12878 and K562 cell lines on two downstream tasks, including the prediction of Hi-C contact maps and chromatin loops, to assess the generalization ability of MIX-HIC. In particular, all the models are trained on one cell line and evaluated on the other. The evaluation results of Hi-C contact map prediction and chromatin loops prediction tasks are shown in Figure 5. We note a decrease in performance when all models are evaluated on external datasets compared to within-dataset testing (see Tables 2 and 3). Nevertheless, MIX-HIC continues to outperform other methods, indicating its strong generalization ability in real-world scenarios.

### 5.4. Ablation Study

The MIX-HIC consists of three fundamental components: the integration of Hi-C contact maps with epigenomic tracks, the proposed cross-modal interaction and cross-modal mapping blocks, and the self-supervised pre-training strategy. We conduct an ablation study to assess their effectiveness. Specifically, we investigate: (1) bimodal versus unimodal representations, (2) the effectiveness of missing modality features complement, and (3) the impact of pre-training versus the absence of pre-training.

The comparison results for three tasks on two datasets are

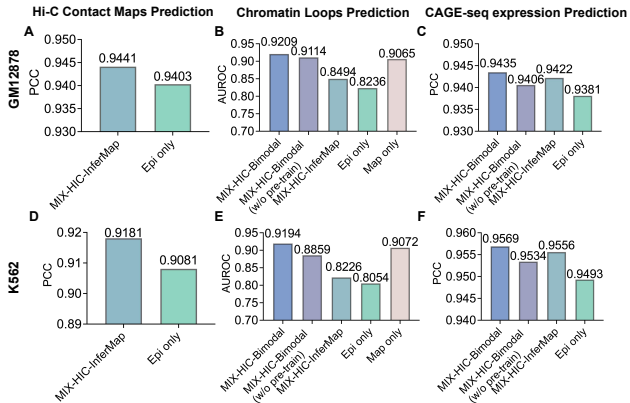


Figure 6. Ablation study results of MIX-HIC for three downstream tasks.

displayed in Figure 6. First, we note that in the chromatin loop prediction task on the K562 dataset, the naive fusion of bimodal representations without loss constraints, denoted as MIX-HIC-Bimodal w/o pre-train, results in performance degradation compared to using the Hi-C contact map alone (referred to as Map only). This may be attributed to the inherent data heterogeneity between the two modalities. With self-supervised pre-training, the integration of both epigenomic tracks and Hi-C contact maps (labeled as MIX-HIC-Bimodal) consistently outperforms the unimodal approach, providing unified and comprehensive representations. Second, MIX-HIC effectively captures the implicit structural connections between bimodal data, demonstrating enhanced performance through the utilization of complementary features (designated as MIX-HIC-InferMap) compared to approaches relying solely on epigenomic tracks (denoted as Epi only). This demonstrates the effectiveness of MIX-HIC in inferring missing features, offering a potential solution to address the data scarcity in 3D genomic studies. Finally, the self-supervised pre-training empowers MIX-HIC to learn a robust and unified representation, achieving superior generalization capability compared to non-pre-trained models.

## 6. Conclusion

In this work, we present MIX-HIC, a novel multimodal foundation model for diverse 3D genome downstream tasks by integrating Hi-C contact maps and epigenomic tracks. To facilitate a unified and comprehensive understanding of 3D genome organization, we constructed the largest paired 3D genome dataset to date, comprising over one million high-quality samples. As the first multimodal foundation model in this domain, MIX-HIC incorporates two key innovations: (1) a cross-modal interaction block that jointly learns modal-invariant and modal-specific representations, effectively capturing both shared and unique biological patterns across modalities; and (2) a cross-modal mapping block that regularizes the multimodal feature space and

enables robust imputation of missing modalities features, alleviating the practical challenges posed by the high costs of Hi-C contact map acquisition. Comprehensive experimental results demonstrate that MIX-HIC achieves state-of-the-art performance on three key downstream tasks across two cell lines. We anticipate this work establishes a new paradigm for multimodal 3D genomics analysis and paves the way for future advancements in the field.

## References

- Avsec, Ž., Agarwal, V., Visentin, D., Ledsam, J. R., Grabska-Barwinska, A., Taylor, K. R., Assael, Y., Jumper, J., Kohli, P., and Kelley, D. R. Effective gene expression prediction from sequence by integrating long-range interactions. *Nature Methods*, 18(10):1196–1203, 2021.
- Beaudry, N. J. and Renner, R. An intuitive proof of the data processing inequality. *Quantum Information and Computation*, 12(5–6):432–441, 2012.
- Chang, J. and Ye, J. C. Bidirectional generation of structure and properties through a single molecular foundation model. *Nature Communications*, 15(1):2323, 2024.
- Chen, T., Kornblith, S., Norouzi, M., and Hinton, G. A simple framework for contrastive learning of visual representations. In *International Conference on Machine Learning*, 2020.
- Cohen, I., Huang, Y., Chen, J., Benesty, J., Benesty, J., Chen, J., Huang, Y., and Cohen, I. Pearson correlation coefficient. *Noise Reduction in Speech Processing*, pp. 1–4, 2009.
- Dong, H., Nejjar, I., Sun, H., Chatzi, E., and Fink, O. SimMDG: A simple and effective framework for multi-modal domain generalization. In *Advances in Neural Information Processing Systems*, 2023.
- Dosovitskiy, A., Beyer, L., Kolesnikov, A., Weissenborn, D., Zhai, X., Unterthiner, T., Dehghani, M., Minderer, M., Heigold, G., Gelly, S., Uszkoreit, J., and Housley, N. An image is worth 16x16 words: Transformers for image recognition at scale. In *International Conference on Learning Representations*, 2021.
- Feng, S., Ni, Y., Li, M., Huang, Y., Ma, Z.-M., Ma, W.-Y., and Lan, Y. Unicorn: A unified contrastive learning approach for multi-view molecular representation learning. *International Conference on Machine Learning*, 2024.
- Ferrer, J. and Dimitrova, N. Transcription regulation by long non-coding RNAs: mechanisms and disease relevance. *Nature Reviews Molecular Cell Biology*, 25(5):396–415, 2024.
- Fudenberg, G., Kelley, D. R., and Pollard, K. S. Predicting 3D genome folding from DNA sequence with Akita. *Nature Methods*, 17(11):1111–1117, 2020.
- Gong, C., Klivans, A., Loy, J. M., Chen, T., Diaz, D. J., et al. Evolution-inspired loss functions for protein representation learning. In *International Conference on Machine Learning*, 2024.
- Hochreiter, S. Long short-term memory. *Neural Computation MIT-Press*, 1997.
- Hsu, C., Verkuil, R., Liu, J., Lin, Z., Hie, B., Sercu, T., Lerer, A., and Rives, A. Learning inverse folding from millions of predicted structures. In *International Conference on Machine Learning*, 2022.
- Karbalayghareh, A., Sahin, M., and Leslie, C. S. Chromatin interaction-aware gene regulatory modeling with graph attention networks. *Genome Research*, 32(5):930–944, 2022.
- Kim, D. and Kim, T. Missing modality prediction for unpaired multimodal learning via joint embedding of unimodal models. In *European Conference on Computer Vision*, pp. 171–187. Springer, 2025.
- Kim, T., Das, D., Choi, S., Jeong, M., Yang, S., Yun, S., and Kim, C. Neural transformation network to generate diverse views for contrastive learning. In *Proceedings of the IEEE/CVF Conference on Computer Vision and Pattern Recognition*, 2023.
- Li, G., Fullwood, M. J., Xu, H., Mulawadi, F. H., Velkov, S., Vega, V., Ariyaratne, P. N., Mohamed, Y. B., Ooi, H.-S., Tennakoon, C., et al. ChIA-PET tool for comprehensive chromatin interaction analysis with paired-end tag sequencing. *Genome Biology*, 11:1–13, 2010.
- Li, S., Wang, Z., Liu, Z., Wu, D., Tan, C., Zheng, J., Huang, Y., and Li, S. Z. VQDNA: Unleashing the power of vector quantization for multi-species genomic sequence modeling. In *International Conference on Machine Learning*, 2024.
- Lieberman-Aiden, E., Van Berkum, N. L., Williams, L., Imakaev, M., Ragoczy, T., Telling, A., Amit, I., Lajoie, B. R., Sabo, P. J., Dorschner, M. O., et al. Comprehensive mapping of long-range interactions reveals folding principles of the human genome. *Science*, 326(5950):289–293, 2009.
- Loshchilov, I. and Hutter, F. Decoupled weight decay regularization. *arXiv preprint arXiv:1711.05101*, 2017.
- Matthey-Doret, C., Baudry, L., Breuer, A., Montagne, R., Guiglielmoni, N., Scolari, V., Jean, E., Campeas, A., Chanut, P. H., Oriol, E., et al. Computer vision for pattern

- detection in chromosome contact maps. *Nature Communications*, 11(1):5795, 2020.
- Monteagudo-Sánchez, A., Noordermeer, D., and Greenberg, M. V. The impact of DNA methylation on CTCF-mediated 3D genome organization. *Nature Structural & Molecular Biology*, 31(3):404–412, 2024.
- Nagelkerke, N. J. A note on a general definition of the coefficient of determination. *Biometrika*, 78(3):691–692, 1991.
- Ramírez, F., Ryan, D. P., Grüning, B., Bhardwaj, V., Kilpert, F., Richter, A. S., Heyne, S., Dündar, F., and Manke, T. deepTools2: a next generation web server for deep-sequencing data analysis. *Nucleic Acids Research*, 44 (Web Server issue):W160, 2016.
- Salameh, T. J., Wang, X., Song, F., Zhang, B., Wright, S. M., Khunsriraksakul, C., Ruan, Y., and Yue, F. A supervised learning framework for chromatin loop detection in genome-wide contact maps. *Nature Communications*, 11(1):3428, 2020.
- Schiff, Y., Kao, C.-H., Gokaslan, A., Dao, T., Gu, A., and Kuleshov, V. Caduceus: Bi-directional equivariant long-range DNA sequence modeling. *International Conference on Machine Learning*, 2024.
- Schwessinger, R., Gosden, M., Downes, D., Brown, R. C., Oudelaar, A. M., Telenius, J., Teh, Y. W., Lunter, G., and Hughes, J. R. DeepC: predicting 3D genome folding using megabase-scale transfer learning. *Nature Methods*, 17(11):1118–1124, 2020.
- Tan, J., Shenker-Tauris, N., Rodriguez-Hernaez, J., Wang, E., Sakellaropoulos, T., Boccalatte, F., Thandapani, P., Skok, J., Aifantis, I., Fenyő, D., et al. Cell-type-specific prediction of 3D chromatin organization enables high-throughput in silico genetic screening. *Nature Biotechnology*, 41(8):1140–1150, 2023.
- Wang, H., Chen, Y., Ma, C., Avery, J., Hull, L., and Carneiro, G. Multi-modal learning with missing modality via shared-specific feature modelling. In *Proceedings of the IEEE/CVF Conference on Computer Vision and Pattern Recognition*, pp. 15878–15887, 2023.
- Wang, S., Zhang, Q., He, Y., Cui, Z., Guo, Z., Han, K., and Huang, D.-S. DLoopCaller: A deep learning approach for predicting genome-wide chromatin loops by integrating accessible chromatin landscapes. *PLoS Computational Biology*, 18(10):e1010572, 2022.
- Wolff, J., Rabbani, L., Gilsbach, R., Richard, G., Manke, T., Backofen, R., and Grüning, B. A. Galaxy HiCEXplorer 3: a web server for reproducible Hi-C, capture Hi-C and single-cell Hi-C data analysis, quality control and visualization. *Nucleic Acids Research*, 48(W1):W177–W184, 2020.
- Yang, M., Zhang, S., Zheng, Z., Zhang, P., Liang, Y., and Tang, S. Employing bimodal representations to predict DNA bendability within a self-supervised pre-trained framework. *Nucleic Acids Research*, 52(6):e33–e33, 2024.
- Yang, R., Das, A., Gao, V. R., Karbalayghareh, A., Noble, W. S., Bilmes, J. A., and Leslie, C. S. Epiphany: predicting Hi-C contact maps from 1D epigenomic signals. *Genome Biology*, 24(1):134, 2023.
- Zhang, Y. and Blanchette, M. Reference panel guided topological structure annotation of hi-c data. *Nature Communications*, 13(1):7426, 2022.
- Zhang, Y. and Blanchette, M. Reference panel-guided super-resolution inference of Hi-C data. *Bioinformatics*, 39 (Supplement\_1):i386–i393, 2023.
- Zhang, Y., Boninsegna, L., Yang, M., Misteli, T., Alber, F., and Ma, J. Computational methods for analysing multiscale 3D genome organization. *Nature Reviews Genetics*, 25(2):123–141, 2024.
- Zhang, Z., Feng, F., Qiu, Y., and Liu, J. A generalizable framework to comprehensively predict epigenome, chromatin organization, and transcriptome. *Nucleic Acids Research*, 51(12):5931–5947, 2023.
- Zhao, H., Dan, C., Aragam, B., Jaakkola, T. S., Gordon, G. J., and Ravikumar, P. Fundamental limits and tradeoffs in invariant representation learning. *Journal of Machine Learning Research*, 23(340):1–49, 2022.
- Zhao, J., Zhuang, W., Song, J., Li, Y., and Lu, S. Pre-training protein bi-level representation through span mask strategy on 3D protein chains. In *International Conference on Machine Learning*, 2024.

## A. Implementation Details.

In this section, we present the implementation details of MIX-HIC, including data source and processing, whole-chromosome loop annotation, as well as experimental settings. Note that we will open-source our code and dataset after the paper publishing.

Table S1. Data sources and accession numbers from 4DN Data Portal and ENCODE Data Portal.

Cell line	Hi-C	DNase-seq	ATAC-seq	ChIA-PET	CAGE-seq
GM12878	4DNFI1UEG1HD	ENCSR000EMT	ENCSR095QNB	ENCSR184YZV	ENCSR000CKA
K562	4DNFITUOMFUQ	ENCSR000EOT	ENCSR956DNB	ENCSR597AKG	ENCSR000CJN
HepG2	4DNFICSTCJQZ	ENCSR000EJV	ENCSR042AWH	ENCSR411IVB	-
HCT116	4DNFIXTAS6EE	ENCSR000ENM	ENCSR872WGW	ENCSR278IZK	-
IMR90	4DNFIH7TH4MF	ENCSR477RTP	ENCSR200OML	ENCSR076TTY	-
WTC11	4DNFIVSCH2CH	ENCSR785ZUI	ENCSR541KFY	ENCSR353ASS	-

### A.1. Data Source and Processing

Detailed reference numbers for all data sources are provided in Table S1. We download the BAM files for epigenomic tracks and convert them into bigWig files using deepTools (Ramírez et al., 2016) with RPGC normalization. Two 250 kb epigenomic regions, corresponding to the x-axis and y-axis of a Hi-C contact map, are first averaged over every 100 bp and transformed using  $\log(x + 1)$  to reduce data variability, and then the processed regions are concatenated to form the final epigenomic tracks input with a length of 5,000. The Hi-C contact maps are binned at 5 kb resolution and normalized using KR normalization, and then divided into  $50 \times 50$  sub-matrices based on the loci of each sample.

The training samples of three downstream tasks are generated using two widely adopted cell lines, GM12878 and K562, as described below. First, the Hi-C contact maps and epigenomic tracks within a 250 kb genomic region upstream and downstream of the gene transcription start site (TSS) are used to predict CAGE-seq expression, with TSS annotations obtained from previous work (Karbalayghareh et al., 2022). For this task, the number of training samples for GM12878 and K562 are 16,046 and 14,739, respectively. Second, the same pairwise samples of Hi-C contact maps and epigenomic tracks are used for the Hi-C contact map prediction task, with the same sample sizes as mentioned above. Third, the positive chromatin loops (1,344,270 for GM12878 and 137,558 for K562) are derived from the ChIA-PET data, while an equal number of negative loops are randomly sampled based on two criteria following prior research (Wang et al., 2022): (1) matching the distance distribution of positive samples using the distances probability density function, and (2) selecting interactions with distances greater than the maximum distance observed in the positive samples to enhance the diversity of the negative samples. Following previous work (Wang et al., 2022; Tan et al., 2023; Yang et al., 2023), we partition the chromosomes into distinct training, validation, and test sets. Specifically, chromosomes 10 and 11 serve as the validation set, chromosomes 3, 13, and 17 as the test set, and the remaining chromosomes are used for model training across three downstream tasks.

### A.2. Whole-chromosome Loops Annotation

The well-trained MIX-HIC model is capable of predicting all potential chromatin interactions across individual chromosomes. The detection of chromatin loops within each chromosome consists of two key steps: (1) scoring potential chromatin interactions using MIX-HIC and (2) aggregating loops through a clustering algorithm. First, candidate elements are identified by examining the diagonals of the raw Hi-C contact matrix, where observed interaction frequencies are statistically compared to expected values based on a Poisson distribution, retaining only elements with p-values below 0.01. Subsequently, the trained MIX-HIC model is employed to predict loop probability scores, with scores exceeding 0.5 referred to as candidate loops. These candidates are further grouped to identify significant loops using a density-based clustering algorithm following (Zhang & Blanchette, 2022). For each candidate, a local density score and a minimum distance metric are computed. Candidates exhibiting low distance values are subsequently eliminated to minimize redundancy. Cluster centers are determined via a target-decoy search, ensuring that the false discovery rate remains below 5%. Within each cluster, the candidate demonstrating the highest local density is designated as the representative loop.

### A.3. Experimental Settings

MIX-HIC is developed using Python and PyTorch, and executed on the Ubuntu platform with a Tesla A100 GPU. MIX-HIC processes input data consisting of  $50 \times 50$  Hi-C contact maps and epigenomic tracks with a sequence length of 5,000 bps. The architecture is composed of feature encoders, task-specific decoders, and a modality fusion block. The feature encoders and task-specific decoders are structured with four layers, each comprising two transformer encoder blocks. Notably, the epigenomic feature encoder includes an additional preprocessing stage, integrating four convolutional layers followed by max-pooling operations before the transformer blocks, to effectively process and condense long sequences. Similarly, the modality fusion block is constructed with two transformer encoder blocks, ensuring efficient integration of features across modalities.

During the pre-training stage, MIX-HIC is configured with 500 epochs, a learning rate of  $1e-5$ , and a batch size of 256. For the CAGE-seq expression prediction task, the predefined feature dimension  $C$  and learning rate are set to 256 and  $1e-4$ , respectively. For the prediction of Hi-C contact maps and chromatin loops, these parameters are specified as 128 and  $1e-5$ , respectively. The number of transformer blocks  $T$  in each encoder, contact map-grounded fusion block, and decoder is set to 2. Fine-tuning is conducted with a batch size of 64, utilizing the AdamW optimizer (Loshchilov & Hutter, 2017) with the momentum parameters  $\beta_1$  and  $\beta_2$  initialized to 0.9 and 0.999, respectively. The fine-tuning process is configured with a maximum of 200 epochs, and an early stopping strategy is employed with a patience parameter of 20 to prevent overfitting.

## B. Analysis of Information Gap Between Bimodal Representations.

Simple alignment of multimodal features can result in information loss, which may compromise the performance of downstream tasks. Under conditions of perfect feature alignment, the prediction error using aligned features is at least  $\Gamma_q$  greater than that using the raw inputs. We generalize the theorem from (Dong et al., 2023) to the case of two modalities as follows.

Let  $q$  represent the joint distribution of  $(z_1, z_2, t)$ , where  $z_1$  and  $z_2$  denote the two modalities, and  $t$  is the target variable. The information gap is formulated as  $\Gamma_q := \max\{U(z_1; t), U(z_2; t)\} - \min\{U(z_1; t), U(z_2; t)\}$ , with  $U(z_j; t)$  representing the mutual information between the target  $t$  and the modality  $z_j$ . The methodology utilizes the cross entropy loss  $\mathcal{L}_{CE}$ , two feature encoders  $f^1(\cdot)$  and  $f^2(\cdot)$ , a feature prediction function  $h(\cdot)$ , and a raw data prediction function  $h'(\cdot)$ . If the bimodal features  $\mathbf{F}^1 = f^1(z_1)$  and  $\mathbf{F}^2 = f^2(z_2)$  are perfectly aligned, *i.e.*,  $\mathbf{F}^1 = \mathbf{F}^2$ , then we can obtain the theorem:

$$\inf_h \mathbb{E}_q[\mathcal{L}_{CE}(h(\mathbf{F}^1, \mathbf{F}^2), t)] - \inf_{h'} \mathbb{E}_q[\mathcal{L}_{CE}(h'(z_1, z_2), t)] \geq \Gamma_q. \quad (9)$$

This theorem implies that if one modality is more informative than the others (*i.e.*, there exists a significant information gap), perfect alignment may lead to a substantial increase in prediction error. The underlying reason is that perfect alignment constrains the aligned features to preserve only the predictive information shared across all modalities, which may result in the loss of modal-specific information that is potentially critical for achieving accurate predictions. The proof of this theorem is presented as follows:

Consider the joint mutual information  $U(\mathbf{F}^1, \mathbf{F}^2; t)$ . Applying the chain rule of mutual information, we obtain:

$$U(\mathbf{F}^1, \mathbf{F}^2; t) = U(\mathbf{F}^1; t) + U(\mathbf{F}^2; t | \mathbf{F}^1) = U(\mathbf{F}^2; t) + U(\mathbf{F}^1; t | \mathbf{F}^2). \quad (10)$$

Under the condition of perfect alignment between the two features,  $U(\mathbf{F}^2; t | \mathbf{F}^1) = U(\mathbf{F}^1; t | \mathbf{F}^2) = 0$ , which implies:

$$U(\mathbf{F}^1, \mathbf{F}^2; t) = U(\mathbf{F}^1; t) = U(\mathbf{F}^2; t). \quad (11)$$

By applying the data processing inequality (Beaudry & Renner, 2012):  $U(\mathbf{F}^1; t) \leq U(z_1; t)$  and  $U(\mathbf{F}^2; t) \leq U(z_2; t)$ , we derive:

$$U(\mathbf{F}^1, \mathbf{F}^2; t) = \min\{U(\mathbf{F}^1; t), U(\mathbf{F}^2; t)\} \leq \min\{U(z_1; t), U(z_2; t)\} \leq \max\{U(z_1; t), U(z_2; t)\} \leq U(z_1, z_2; t). \quad (12)$$

According to the variational form of conditional entropy  $H(t|z_1, z_2) = \inf_h \mathbb{E}_q[\mathcal{L}_{CE}(h(z_1, z_2), t)]$  (Zhao et al., 2022) and

the definition of mutual information  $U(X; Y) = H(Y) - H(X|Y)$ , we can conclude the theorem as follows:

$$\begin{aligned}
 \inf_h \mathbb{E}_q[\mathcal{L}_{\text{CE}}(h(\mathbf{F}^1, \mathbf{F}^2), t)] &= \inf_{h'} \mathbb{E}_q[\mathcal{L}_{\text{CE}}(h'(z_1, z_2), t)] \\
 &= H(t|\mathbf{F}^1, \mathbf{F}^2) - H(t|z_1, z_2) \\
 &= H(t) - U(\mathbf{F}^1, \mathbf{F}^2|t) - (H(t) - U(z_1, z_2|t)) \\
 &= U(z_1, z_2; t) - U(\mathbf{F}^1, \mathbf{F}^2; t) \\
 &\geq \Gamma_q.
 \end{aligned}$$

Therefore, although perfect alignment of bimodal features achieves consistency, it risks losing critical modal-specific information, potentially leading to higher prediction errors, especially when the information gap between modalities is substantial, as seen in the case of Hi-C contact maps and epigenomic tracks. To solve this problem, we introduce cross-modal interaction and cross-modal mapping blocks to capture both modal-invariant and modal-specific features, enabling a more comprehensive representation of bimodal data. The effectiveness of this approach is validated through extensive ablation studies.

## C. Additional Experimental Results.

### C.1. Proportion of Validated Loops versus Predicted Loops

Table S2 presents a comparative analysis of chromatin interaction loops identified through ChIA-PET experiments and those predicted by different approaches.

Table S2. Comparison of ChIA-PET-supported loops with those identified by various deep learning methods.

Methods	GM12878			K562		
	Validated Loops	Predicted Loops	Proportion	Validated Loops	Predicted Loops	Proportion
HiCEXplorer	1358	2688	0.51	765	1450	0.53
ChromoSight	3845	6044	0.64	1247	1963	0.63
Peakachu	1992	2904	0.69	718	1221	0.59
DLoopCaller	3849	6019	0.64	1048	2274	0.46
MIX-HIC	5179	5893	0.88	1064	1588	0.67

### C.2. Example of Whole-Chromosome Chromatin Loop Comparison

Figure S1 illustrates the performance evaluation of chromatin loops predicted by various methods (black points, lower left) against experimentally validated interactions (red points, upper right). Our predictions (the first left panel of Figure S1) demonstrate significantly fewer false positive loops compared to experimentally validated ChIA-PET interactions in the Chromosome 13 region (20Mb-22Mb) from the GM12878 dataset, as evidenced by the correspondent counts between red and black points. The comparative visualization highlights the enhanced specificity of our approach in identifying chromatin interactions across the genomic region of interest.

### C.3. Hyperparameter Analysis

The number of Transformer  $T$  blocks in each layer of the encoder, contact map-grounded fusion block, and decoder, along with the predefined feature dimension  $C$  play a pivotal role in MIX-HIC. We evaluate the impact of this parameter by testing  $C = \{64, 128, 256\}$  and  $T = \{2, 4, 8\}$  as depicted in Figure S2 and Figure S3, respectively. The highest performance is achieved at  $C = 128$  for HI-C contact maps and chromatin loops prediction tasks, while  $C = 256$  performs best for CAGE-seq expression prediction. Additionally,  $T = 2$  demonstrates the most robust performance across all three downstream tasks. MIX-HIC exhibits strong resilience to parameter variations, underscoring its robustness. These experimental results substantiate the parameter configurations employed in MIX-HIC.

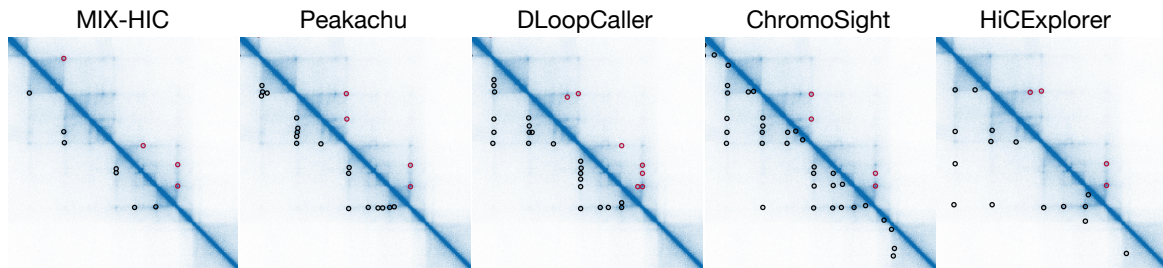


Figure S1. Comparison of predicted chromatin loops (black points, lower left) and experimentally validated ChIA-PET interactions (red points, upper right) in the Chromosome 13 region (20Mb-22Mb) from the GM12878 dataset.

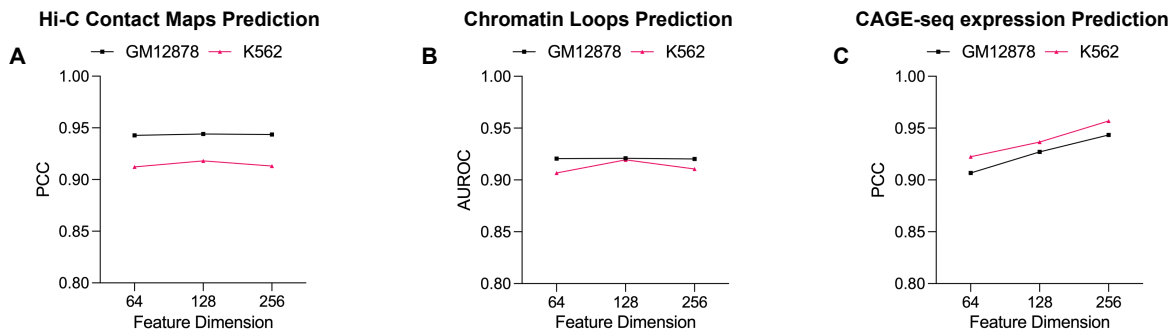


Figure S2. The performance across different predefined feature dimensions  $C = \{64, 128, 256\}$  for three downstream tasks in GM12878 and K562 cell lines.

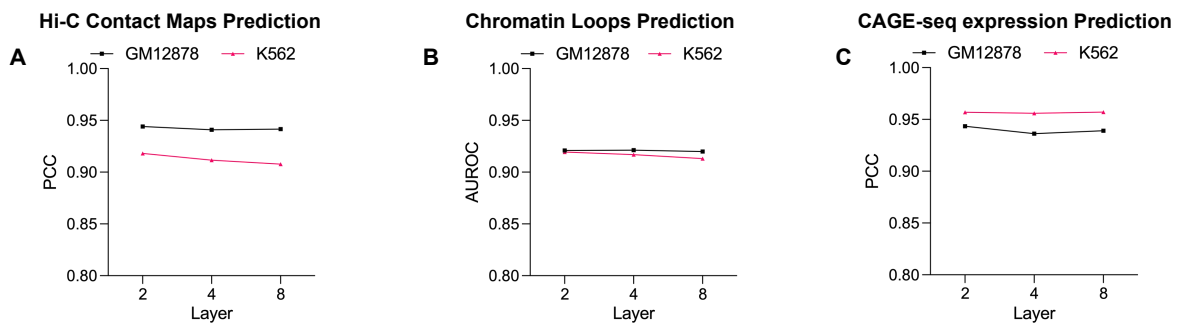


Figure S3. The performance across different Transformer layer  $T = \{2, 4, 8\}$  for three downstream tasks in GM12878 and K562 cell lines.